Journal of Power Sources 268 (2014) 658–669

Contents lists available at ScienceDirect

Journal of Power Sources

journal homepage: www.elsevier.com/locate/jpowsour

A comparative study of commercial lithium ion battery cycle life in electric vehicle: Capacity loss estimation

Xuebing Han, Minggao Ouyang*, Languang Lu, Jianqiu Li

Department of Automotive Engineering, State Key Laboratory of Automotive Safety and Energy, Tsinghua University, Beijing 100084, PR China

HIGHLIGHTS

- A dynamic cycle life experiment is designed according to the EV application and five different cells are tested.
- Capacity loss is simulated using a semi-empirical model based on the experiment results and identified aging mechanism.
- An on-board battery capacity loss estimation method is proposed.

ARTICLE INFO

Article history:
Received 23 December 2013
Received in revised form
8 June 2014
Accepted 19 June 2014
Available online 26 June 2014

Keywords:
Lithium ion battery
Electric vehicle
Capacity loss model
Cycle life
State of health

ABSTRACT

Now the lithium ion batteries are widely used in electric vehicles (EV). The cycle life is among the most important characteristics of the power battery in EV. In this report, the battery cycle life experiment is designed according to the actual working condition in EV. Five different commercial lithium ion cells are cycled alternatively under 45 °C and 5 °C and the test results are compared. Based on the cycle life experiment results and the identified battery aging mechanism, the battery cycle life models are built and fitted by the genetic algorithm. The capacity loss follows a power law relation with the cycle times and an Arrhenius law relation with the temperature. For automotive application, to save the cost and the testing time, a battery SOH (state of health) estimation method combined the on-line model based capacity estimation and regular calibration is proposed.

1. Introduction

The EVs are developing very fast nowadays. The batteries are among the most critical parts of the EV and the lithium ion batteries are widely accepted as the best choice owing to such factors as their high energy density and power density, environmental friendship, long cycle life and calendar life, etc. The cycle life is one of the most significant characteristics for power batteries in EV [1].

From an automotive engineer's perspective, there are only two things need to be known about the batteries: how much power the battery system could supply, and how much energy is stored in the battery system. It is simpler to estimate the results of these two questions for a new cell, but for an aged cell, there would be large estimation error without knowing the amount of battery capacity loss. Thus, the battery capacity loss modeling and estimation are very important. With a precise capacity loss model, the battery management system could make an accurate estimation of the battery capacity and derive the batter SOH (state of health). And then all the other battery management algorithm would get better results.

The cycle life of batteries with different cathode and anode materials are different. At present, the positive electrode materials used in commercial lithium ion batteries mainly include $LiMn_2O_4$ (LMO), $LiFePO_4$ (LFP), $LiNi_xCo_yMn_{1-x-y}O_2$ (NCM), etc., and the most commonly used negative electrode material is Carbon (C). In recent years, the lithium ion batteries with $Li_4Ti_5O_{12}$ (LTO) as the negative electrode material are developing very rapidly and the LTO is currently regarded as one of the promising choice to be used in lithium ion batteries instead of the carbon based anode material owing to its excellent performance under low temperature, long cycle life, etc [2,3].

The battery life includes calendar life and cycle life. In this study, we focused only on the cycle life of lithium ion batteries. As the

* Corresponding author. Tel.: +86 10 62792797; fax: +86 10 62789699.
E-mail address: ouymg@tsinghua.edu.cn (M. Ouyang).

http://dx.doi.org/10.1016/j.jpowsour.2014.06.111
0378-7753/

cycle life of batteries is influenced by many factors such as temperature, SOC (State of charge), ΔSOC, charge and discharge current, charging cut-off voltage and discharging cut-off voltage, charging method, etc., different researchers design different battery cycle life test profiles as a result of different research objectives.

For instance, P. Ramadass et al. [4] investigate and compare the cycle life of batteries at room temperature, 45°, 50° and 55°. And Sheng Shui Zhang [5] investigates how three different charging methods, including CCCV, constant power–constant voltage (CPCV) and multistage constant current–constant voltage (MCCCV) charging methods, affect the cycle life of batteries. And Soo Seok Choi et al. [6] investigates the influence on the battery cycle life of charge cut-off voltage, discharge cut-off voltage, constant voltage charging time, charging current, discharging current, etc., respectively. Jiuchun Jiang et al. [7] investigate the long term cycling performances of $LiFePO_4$/graphite batteries in different SOC ranges.

The above literature design cycle life test to find the influence of separate factors on the cycle life of batteries respectively, which means in each group of tests only one factor is involved. There are also some literature which investigate the impact of multiple factors on the cycle life of batteries, which means the coupling of different factors is also investigated. For instance, I. Bloom et al. [8,9] take $LiNi_{0.8}Co_{0.2}O_2$/C batteries as research object, conduct the durability test of batteries of different SOC of 80% and 60%, with different ΔSOC of 3% and 6% and under different temperatures including 40 °C, 50 °C, 60 °C and 70 °C. And John Wang et al. [10] conduct the battery durability test at different temperatures (−30 °C, 0 °C, 15 °C, 25 °C, 45 °C and 60 °C), different ΔSOCs (90%, 80%, 50%, 20% and 10%), different charge and discharge rates (1/2 C, 2 C, 6 C, 10 C). The test costs huge manpower and material resources, and it requires long test duration for the cycle life test and large amount of batteries required for experiment, since that every possible combination of different levels of different factors should be tested.

There are also some researchers design the battery cycle life test according to the vehicles in which the batteries would be used. At present, there have been many hybrid electric vehicles (HEV) in the market like Prius, Volt, etc. Thus there have been some literature which have made profound researches on the cycle life of lithium ion batteries for HEV. For instance, for some commonly HEV, the batteries tend to be charged and discharged at a specific SOC and a small ΔSOC. J. Belt et al. [11] designed a special working cycle for life test according to the actual working condition of HEV and test the cycle life of batteries under temperature of 40 °C and the batteries are cycled between SOC about 60%–80%, 45%–65% and 30%–50%, respectively.

For plug-in hybrid electric vehicles (PHEV), the batteries would be working under different working conditions depend on the different control strategies. Currently the control strategy commonly used in PHEV is CDCS strategy (charge-depleting, charge-sustaining), that means, batteries work first in CD mode until the SOC reaches a certain set value, then work in CS mode. M. Ecker et al. [12] taking NCM/C batteries and LMO/C batteries as research object, conduct CD cycle test, CS cycle test of batteries respectively under different temperatures of 40 °C, 50 °C, 60 °C and 70 °C.

At present, based on the cycle life experiment results, research on capacity loss modeling of lithium ion batteries mainly includes capacity loss modeling based on the battery aging mechanism, and some researchers build empirical or semi-empirical capacity loss models based on the battery cycle test results under different cycle parameters.

For lithium ion batteries with carbon anode, one of the most important aging mechanism is the loss of lithium ions caused by the formation and continuous thickening of SEI (Solid Electrolyte Interface) film on the surface of anode particle. Based on this principle, the capacity loss models could be built and are studied in many literature [13,14]. The stress due to the lithium ion insertion/extraction of the electrode particles is also one important aging mechanism. R. Deshpande [15] introduces the capacity loss model based on the SEI formation and the mechanical fatigue caused by the diffusion induced stress in the carbon anode particle. Y. Dai [16] introduces a mathematical model to simulate the stress in the LMO cathode particle. For lithium ion batteries with LMO cathode, a capacity fade model considering the manganese (Mn) dissolution is built by R.E. White [17]. However, mechanism models are very complicated, many parameters and massive calculation are involved. Meanwhile, usually the mechanism model can only focus on one or two certain side reactions which affect the battery life, and various side reactions are still unknown or very hard to be investigated and considered in the mechanism model. Thus, the mechanism model may be impossible to accurately reflect the battery aging, especially under the real working conditions which are usually very complicated and different from the cycling conditions of the experiment in labs. Thus it is quite hard to employ the mechanism model in the BMS (battery management system) of vehicles. However, the battery aging mechanism could be utilized to guide the semi-empirical capacity loss model development.

There are already some researches on the semi-empirical models of lithium ion batteries cycle life. The related literature [11,18–20] etc., point out that a power law exists between the battery capacity loss and the cycle numbers. N. Omar [21] introduces a complicated capacity loss model considering the influence of the working temperature, charge and discharge rate, depth of discharge. In our previous work [22], capacity loss model considering the temperature, charge and discharge rate, end of charge and discharge voltage is built. Though the aging mechanism is not considered, now the empirical models can be used to find the battery capacity loss under different cycling conditions and are easier to be applied in BMS for predicting the battery capacity fades because fewer parameters are involved and the calculation would be simple. Thus in this paper, the battery capacity loss would be fitted by a semi-empirical model.

However, in all these researches, a lot of cells would be cycled with different cycle parameters, i.e., under different temperatures or with different charge/discharge rates, many cells and long testing times are needed, but for a certain cell, the cycle parameters are constant. Nevertheless, in a real vehicle the cells would be continuously working under various conditions, so the semi-empirical model introduced in the former works could not be directly used in the BMS. Thus, in this study, the semi-empirical model would be developed according to the aging mechanism and then transformed to a discrete version. The aging mechanism identification of all the cells used in this study has been shown in our previous work [23].

Considering that in real EV, the battery working condition changes, especially the ambient temperature changes with the seasons, in this study, five different commercial lithium ion cells would be cycled under a specific cycle with dynamic temperatures. The experiment design is shown in Section 2. Based on this particular experiment, only one cell is tested and the capacity loss model could be built. Thus huge time and cost could be saved. The capacity loss model parameter fitting by genetic algorithm is shown in Section 3. For the real automotive application, to save time and improve the capacity estimation precision, a battery SOH (state of health) estimation method combined the on-line model based capacity estimation and regular calibration is proposed in Section 4. And the conclusion is shown in Section 5.

Table 1
Basic parameters of the five cells.

	Cathode material	Anode material	Rated capacity (Ah)
A	NCM	LTO	20
B	LFP	C	60
C	LFP	C	11
D	LMO	C	35
E	LMO	C	10

2. Experiment

In this study, five commercial lithium ion cells from different manufactures are selected, conduct the cycle life test. All these cells are candidates for an EV application. For convenience, five batteries are labeled as cell A, B, C, D and E. The basic parameters of these five cells are shown in Table 1. Such five cells cover basically the mainstream types of lithium ion power batteries for EV application in the current battery market.

The experiments are conducted in an 8-channels, UBT 100-020-8 type battery test bench made by DIGATRON which has a current range of −100A to +100 A and a voltage range of 0 V–20 V. The voltage accuracy is 1 mV and the current accuracy is ±0.1% full scale. All the five tested battery cells are put into one temperature chamber to keep the ambient temperature of the cell under a same specific and constant value. The temperature chamber is from Dongguan Bell Company and the type is BE-TH-150M3.

2.1. Reference performance test (RPT)

The battery RPT mainly includes capacity test and Hybrid Pulse Power Characterization (HPPC) test of batteries. As the capacity of batteries fades and the resistance increases with increasing cycle number, an RPT test is not only required for new batteries to determine their performance, but it also is required after every 30 cycles during the battery cycle test in order to determine the capacity and resistance of the batteries so as to obtain the degradation of battery performance with increasing cycle number.

The battery capacity test is designed to find the battery standard capacity. Put the battery in the temperature chamber under 25 °C for 3 h; then discharge the battery at constant discharge current 1/3 C to the discharge cutoff voltage, pause 1 h for the battery internal relaxation and diffusion process, and then fully charge the battery and another 1 h pause. This process could be repeated 4 times and the mean value of the discharge capacity would be taken as the battery capacity. In this study, the battery charging method is referred to the manufacturer's recommended charging algorithm. The constant current–constant voltage (CCCV) charging method is used, which means constant current (1/3 C) charging until the voltage gets to the charge cutoff voltage, then constant voltage charging until the charging current falls below 0.05 C.

The HPPC test is designed to find the open circuit voltage (OCV) and resistance characteristics. Base on the HPPC test, the battery power capability could be calculated, and it is also helpful to build the battery model.

The HPPC test consists of a sequence of several HPPC profiles [24] at different selected SOC (state of charge), constant current (CC) discharge to adjust the battery SOC to the selected value and some pause for the battery relaxation process. The HPPC profile introduced is shown in Fig. 1. Consider that the battery is to be used in EV, the HPPC profile is consisted of 30 s discharge, 40 s pause and 10 s charge [25].

2.2. Design of the cycle life test

At present there are few literature which intend to design battery cycle life for pure EV. That is probably because there are not many commercial pure EV at present and the pure EV works under a relatively simple working condition. Moreover, in the existing cycle life researches, different batteries may cycle under different working conditions but for every battery the cycle condition is unchanged. However, in real vehicles, the batteries certainly work in a changing condition instead of an unchanged cycle condition. Especially the battery would never working under a constant environment temperature because of the changing of seasons. On the basis of the considerations mentioned above, the battery cycle test was designed as follows.

Compared with HEV, pure EV has a much simpler cycle working condition. A typical driving cycle for a pure EV may be like this: charging the battery in the night, and driving inside the city to the work place or to downtown, then driving back home and charging. In normal conditions, when the batteries are charged slowly following the standard charging method at night or in a parking lot, the charging current is always small and constant; when the vehicle is running, the discharging current tends to be consistent as the batteries are required to supply all the driving power. This is quite different from batteries in HEV working with large charge and discharge pulses. As a result, in the process of cycle life test, we choose the charge rate 0.3 C to charge cells until the voltage reach the charge cut-off voltage, pause for 20 min, then discharge the

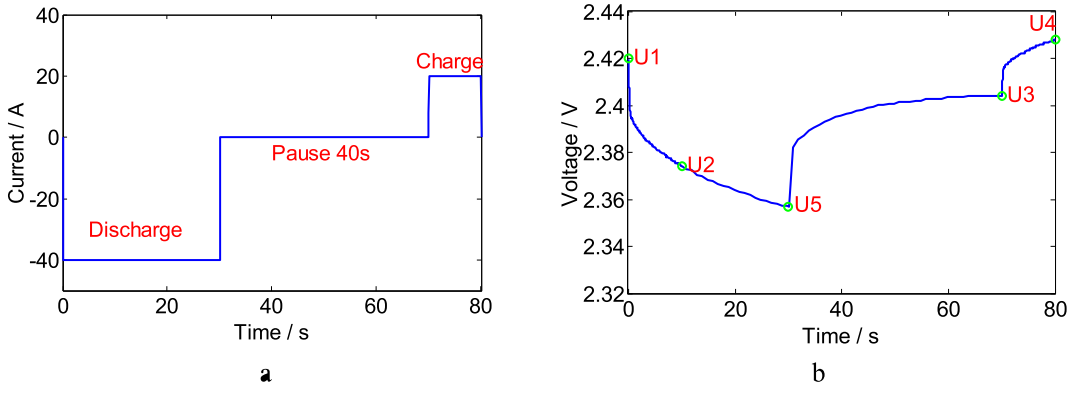

Fig. 1. The HPPC profile (cell A), a. The HPPC current profile, b. The HPPC voltage profile (new battery, SOC = 0.7).

cells at 1.5 C until the voltage reach the discharge cut-off voltage, pause for 20 min and continue to cycle the battery charging and discharging as above.

On a real vehicle, the battery working temperature will change because of the alternating seasons. For HEV, the battery temperature rises fast as the batteries are always charged and discharged frequently with high charge and discharge rate. And even in winter, the battery could also be warmed by means like the engine exhaust heating. The result is that usually the battery temperature in HEV keeps on a very high value. Consequently, elevated temperature is always chosen for cycle life test of HEV batteries. For example, the testing temperature of the literature [11,12] is above the room temperature 25 °C. But for the EV batteries, there are some differences. In summer, the temperature of batteries is always higher because of the high environment temperature and the Joule-heat generated from battery charging and discharging; in winter, the temperature of batteries is always lower because of the low environment temperature, and the Joule-heat could not heat the batteries to very high temperature since for EV batteries the charge and discharge rate is usually not very high. Thus, actual working temperatures of batteries for EV tend to differ in winters and in summers. In order to ensure the performance and the life of batteries, the present BMS is often equipped with some facilities for battery heat management, for example, fan, heating wire, etc., to guarantee that the temperature of batteries could stay within a reasonable range. However, such method cannot ensure that the batteries work at standard 25 °C in both winters and summers. For the purpose of simplifying this process and for convenience of testing in the laboratory, the batteries are cycled alternately in the environments at 45 °C and 5 °C. Cycling at 45 °C represents the high working temperature of batteries in summers and cycling at 5 °C represents that although the external temperature is possible to be very low, even at −20 °C in winters, the electric vehicle shall be equipped with appropriate battery heat management system to keep the battery temperature at about 5 °C to guarantee the necessary performance of batteries, especially for LFP and LMO batteries with graphite anode as they are unsuitable for charging at temperature below zero.

Consider that the EV may not be used every day in normal conditions, and suppose the EV is used for 15 times per month and thus its batteries will be fully charged and discharged for about 90 times every half a year. So the batteries cycle life experiment is designed to cycle for 90 times at 45 °C and 90 times at 5 °C, and then continues to repeat such cycles. For former researches, to study the influence of temperature on the capacity loss, more than 3 cells would be tested and cycled under different temperature, and in this study using this specific cycles, only one cell need to be tested. And it would be introduced in Section 3 that the capacity loss model could be determined by the test results of only one cell. So, compare to the former researches, the experiment designed here could save test cells and test time, and it is typically useful to compare the cycle life of various type of batteries.

In order to make a comprehensive investigation of the performance changes of cells, in the cycle test, after every 30 cycles the cells are required to regulate the temperature to 25 °C and conduct one RPT test.

To sum up, the test scheme of durability cycle is designed as shown in Fig. 2.

3. Capacity loss modeling

3.1. Comparison of capacity loss

The capacity here means the standard capacity tested by the RPT under 25 °C and 1/3 C discharge rate. And the following marks are given for the convenience of the discussion below. Mark the capacity of batteries after n cycles as C_n. As the capacity test of batteries is taken after every 30 cycles in the cycle life test process, the battery cycle number before the pth capacity test may be marked as n_p. Thus it could be easily seen that $n_{p+1} = n_p + 30$, $n_0 = 0$.

Since the nominal capacity of different cells is quite different, and for better comparison of capacity loss of different cells, the relative capacity is used. The cell relative capacity could be calculated by Eq. (1).

$$C_{\text{relative},n_p} = \frac{C_{n_p}}{C_{n_0}} \tag{1}$$

where C_{n_p} represents the capacity of current cells, C_{n_0} represents the initial capacity of cell before cycle test, and C_{relative,n_p} represents the relative capacity of current cells. Then the relative capacity loss of batteries, marked as ξ, with unit of %, is shown in Eq. (2).

$$\xi_{n_p} = 1 - C_{\text{relative},n_p} \tag{2}$$

The relative capacity of different cells after different cycle numbers are shown in Fig. 3. From Fig. 3 it can be seen that after 1020 cycles, the standard capacity of LTO cell A shows little capacity loss. The capacity loss of LFP cell B and LFP cell C is of the same order, to be specific, the standard capacity of cell B fades to 78.7% of its initial capacity and capacity of cell C fades to 85.71% of its initial capacity. The standard capacity of LMO cells, i.e., cell D and cell E, fades very quickly. The capacity of cell D fades to 75.18% of its initial capacity after 240 cycles; and the capacity of cell E fades to 78.57% of its initial capacity after 420 cycles. Generally the battery is considered to reach its end of life (EOL) when the battery capacity fades to 80% of its initial value. So LMO cell D and cell E reach their EOL after less than 500 cycles and cannot be used any more. LFP cell B reaches its EOL after about 1000 cycles. LFP cell C would reach its EOL after another 500 cycles. LTO cell A shows unobvious capacity fades and its life would be as long as thousands of cycles.

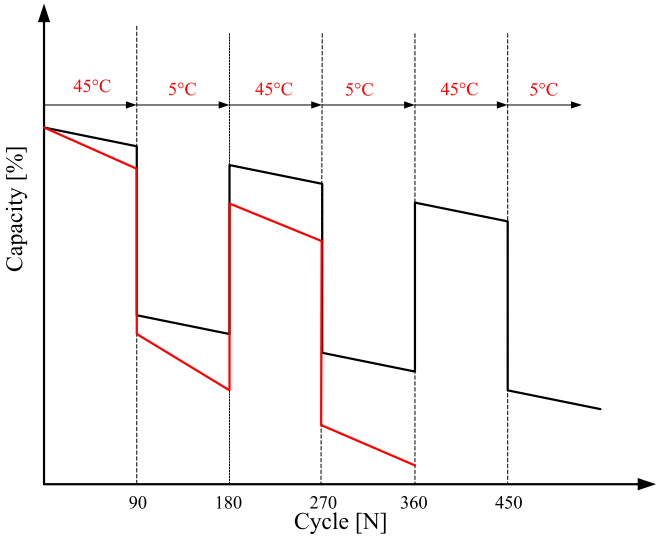

Fig. 2. The cycle life test design.

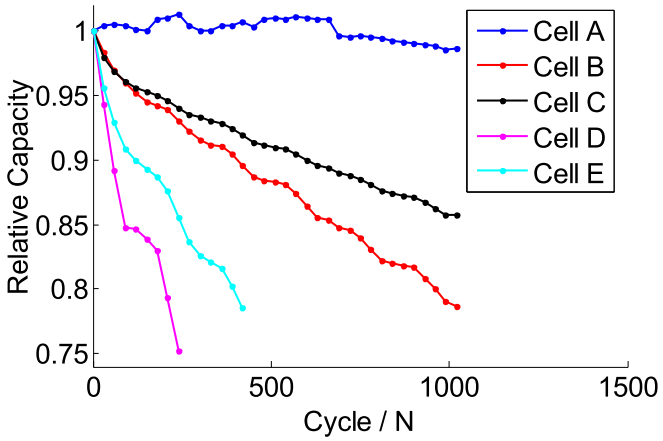

Fig. 3. The relative capacity of all the 5 cells.

The cell relative capacity loss of every 30 cycles $\Delta\xi_{n_p}$ is defined by Eq. (3).

$$\Delta\xi_{n_p} = \xi_{n_p} - \xi_{n_{p-1}} = C_{\text{relative},n_{p-1}} - C_{\text{relative},n_p} \tag{3}$$

From Eq. (3) it could be easily found that $\Delta\xi_{n_p}$ represents the capacity change of batteries before and after the corresponding 30 cycles. Positive $\Delta\xi_{n_p}$ indicates that the capacity of batteries fades after 30 cycles and the bigger $\Delta\xi_{n_p}$ is, the greater the battery capacity loss is; negative $\Delta\xi_{n_p}$ indicates that the capacity of batteries increases after the corresponding 30 cycles. This cell relative capacity loss partially represents the battery capacity fade rate. The relative capacity loss of every 30 cycles of each cell are plotted in Fig. 4. It is clear that before 600 cycles, after every 30 cycles the capacity loss of cell A seems fluctuate up and down around 0 basically, thus the cell capacity shows little capacity loss during the first 600 cycles. After 600 cycles, the relative capacity loss of every 30 cycles is basically a constant positive value and the battery begins to show stable capacity fades but still with slight fade rate. Other types of cells show obvious capacity fades. The capacity loss due to the cycling at 45 °C is higher and at 5 °C is lower. The capacity loss of LMO cells at high temperature (45 °C) is much higher than the LFP cells, while cycling at 5 °C, the capacity fade rate of LMO cells and LFP cells are of the same order. What's more, the capacity fade rate of LFP and LMO cells seems to become lower with the cycle time increases.

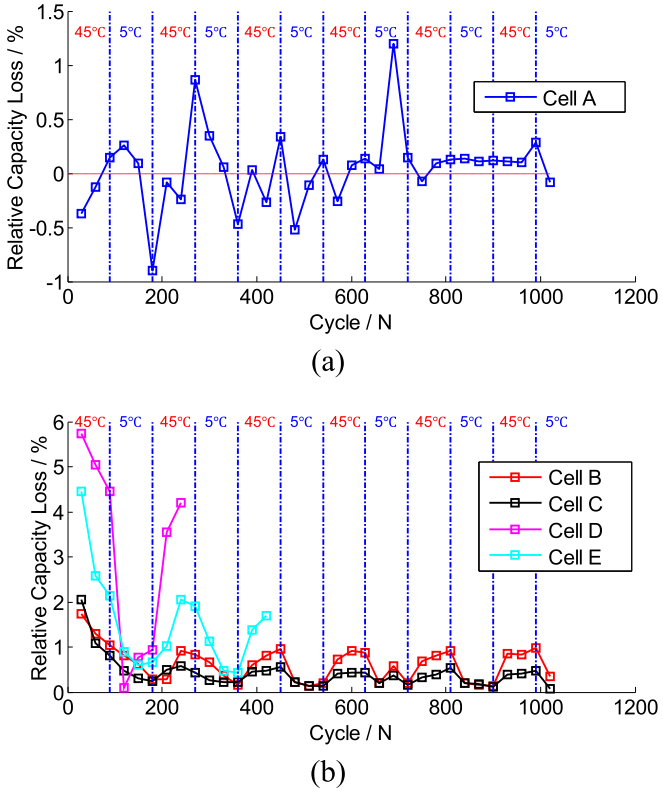

Fig. 4. Relative capacity loss of each 30 cycles. (a), cell A, (b), cell B, C, D, E.

As the cell A shows almost no capacity fade and capacity loss tendency, it is impossible to model its capacity loss and thus further continuous test and efforts are still required. And other cells have shown obvious trend of capacity fades, and their capacity loss would be modeled in Section 3.2.

3.2. Battery capacity loss modeling

In this section, a semi-empirical model for capacity loss of cells would be built based on the battery capacity loss obtained from the RPT and the battery aging mechanism. The battery aging mechanism could be identified by in-situ voltage measurement methods, such as incremental capacity analysis and differential voltage analysis. The detailed analysis of the battery aging mechanism identification has been shown in our previous work [23] and here only the identified results would be shown.

The main aging mechanism for LTO/NCM cell A is the loss of cathode material. For lithium ion cells with carbon based anode, i.e. the C/LFP cell B, cell C, C/LMO cell E, the main aging mechanism is the loss of the usable lithium ions. And for cell B the loss of cathode material is obvious. For cell E there is also some loss of active material. For cell D, the battery aging is mainly caused by the dramatic resistance increase. The loss of lithium ions is usually caused by the formation and thickening of the SEI film. It is widely accepted that the film thickness is proportional to the square root of time, i.e. $t^{1/2}$, and so is the capacity loss, especially for the calendar life [15].

Here consider the main aging mechanism is the lithium ion loss, the capacity loss would be considered to follow a power law relation with the cycle times. And it is widely accepted that, for most chemical process, the influence of temperature on the reaction rate follows the Arrhenius law. Thus, the influence of temperature on capacity loss could also be modeled by this Arrhenius law. So in this case, the battery capacity loss could be described by the Eq. (4).

$$\xi = Ae^{-\frac{E_a}{RT}} \cdot n^z \tag{4}$$

where ξ represents the relative capacity loss of batteries with unit of %, A is a constant, E_a represents the activation energy in J mol^{-1}; R is the gas constant with unit of J/(mol^{-1} K); T represents temperature with unit of K; n represents the cycle numbers and z is the power law factor. Similar models are also used in other literature [18,19] to describe the battery capacity loss. Here it should be noticed that since the loss of lithium ions is not the only aging mechanism, the power law factor z would not be 1/2.

For the battery cycling under an unchanged working conditions, the model parameters A, E_a/R and z could be directly obtained by curve fitting. And then this equation could be directly used to find the battery capacity loss under an unchanged working condition. However, for the experiment designed in this study, the cells are cycled under a dynamic conditions, to be specific, under alternated temperature. Thus the model parameters could not be fitted directly. And it is clear that the batteries in EV are impossible to keep charging and discharging under the same working condition. As a result, it is not practical to directly use the Eq. (4) to predict the battery capacity loss in the real EVs. Thus, this equation should be transformed to a discrete version.

According to the Eq. (4), it can be obtained that

$$n = \left(\xi e^{\frac{E_a}{RT}}/A\right)^{\frac{1}{z}}. \tag{5}$$

By getting derivative of Eq. (4), it could be easily known that

$$\xi' = zAe^{-\frac{E_a}{RT}}n^{z-1} = zAe^{-\frac{E_a}{RT}}\left(\xi e^{\frac{E_a}{RT}}/A\right)^{\frac{z-1}{z}}. \tag{6}$$

That means

$$\xi' = zA^{\frac{1}{z}}e^{-\frac{E_a}{zRT}}\xi^{\frac{z-1}{z}} = k_1 e^{\frac{k_2}{T}}\xi^{k_3}. \tag{7}$$

Then we have:

$$\xi_{n_p} = \xi_{n_{p-1}} + (n_p - n_{p-1})k_1 e^{\frac{k_2}{T}}\xi_{n_{p-1}}^{k_3} \tag{8}$$

where ξ_{n_p} represents the cell capacity loss after n_p times of cycles. k_1, k_2 and k_3 are all constants, and could be calculated by Eq. (9).

$$\begin{cases} k_1 = zA^{\frac{1}{z}} \\ k_2 = -\dfrac{E_a}{zR} \\ k_3 = \dfrac{z-1}{z} \end{cases} \tag{9}$$

Eq. (8) is directly derived from Eq. (4). To be strict, it works only upon the unchanged cycle conditions. To further investigate the capacity loss under the alternate cycle conditions, it could be assumed that Eq. (8) also works as well in the case of changing cycle conditions by reference to the theory of accumulated damage [26], i.e., after n_p cycles, the battery capacity loss is known as $\xi_{n_{p-1}}$, after some additional cycles, the battery capacity loss ξ_{n_p} meet the Eq. (8) and could be derived by the Eq. (8), the additional capacity loss is only depends on the additional cycles, no matter how the battery capacity fades to $\xi_{n_{p-1}}$.

For a new cell, the capacity loss is 0. And the Eq. (8) could not be used to calculate the battery capacity loss. The model initial value could be derived by Eq. (10).

$$\xi_{n_1} = Ae^{-\frac{E_a}{RT}}n_1^z \tag{10}$$

Eqs. (8) and (10) describe the battery capacity loss. The model parameters could be derived by multiple regression. And here another method using genetic algorithm will be shown. For convenience, take $n_1 = 1$, $n_{p+1} = n_p + 1$. And the cell capacity loss could be modeled as Eq. (11).

$$\begin{cases} \xi_1 = Ae^{-\frac{E_a}{RT}} \\ \xi_{n+1} = \xi_n + k_1 e^{\frac{k_2}{T}}\xi_n^{k_3} \end{cases} \tag{11}$$

Given different values of A, E_a/R and z, the estimated battery capacity loss $\tilde{\xi}$ after different cycles could be calculated by Eq. (11). And the temperature should be carefully treated because the battery working temperature changes after every 90 cycles. Since only the capacity of the new cell and cell after every 30 cycles up to 1020 cycles is tested during the life test, the rooted mean squared error (RMSE) between the predicted battery capacity and the tested battery capacity after these cycles could be calculated and shown in Eq. (12).

$$\begin{aligned} &\mathrm{RMSE} = \frac{1}{34}\sum_{n=\,n_0}^{n_{34}}\left(\xi_n - \tilde{\xi}_n\right)^2 \\ &n_0 = 0,\ \ n_{p+1} = n_p + 30. \end{aligned} \tag{12}$$

The RMSE could be selected as the objective function. Using the genetic algorithm to minimize the RMSE, and then the optimal values of A, E_a/R and z could be derived. The modeling results obtained are shown in Table 2 and Fig. 5.

The simulated capacity loss results are very close to the experiment results, indicating that the accumulated damage assumption is acceptable for the cells tested in this study.

And it can be seen that the two LMO cells have relatively approximate and high value of E_a/R, about 1550 to 1600. The two LFP cells have relatively approximate value of E_a/R, about 1300–1,400, comparatively low. The value of A of LMO cells is also higher than that of LFP cells, to be specific, for LMO cells, A is about 0.50–0.65 and for LFP cells is about 0.15–0.2. The coefficient z of all the cells is from 0.58 to 0.76 basically, different from 0.5.

And it is interesting that the aging mechanism of cell C is only the loss of lithium ion, and the z value is the closest to 0.5. The aging mechanism of cell B and cell E is the loss of lithium ion coupled with the loss of active material [23,27], and the z value is higher than that of cell A. The main aging mechanism of cell D is the resistance increases, the influence of lithium ion loss is relatively small, and the z value is the farthest from 0.5. This phenomenon also verifies the fitted results.

4. Battery capacity loss on-board estimation

From an automotive engineer's perspective, the battery capacity loss on-board estimation is more important than the capacity loss model. In the BMS, with accurate battery capacity estimation, the battery SOH would be derived, and the precision of SOC estimation could be improved, and the SOH is also an important parameter for the management algorithm of the batteries and the vehicle [1].

Some literature [28,1] have mentioned some battery parameter on-line estimation method like dual Kalman filtering, to estimate the battery capacity and resistance in real time. The

Table 2
Parameters of the cycle life models of different cells.

Cell	A	E_a/R	z
B	0.1549	1430.35	0.7151
C	0.1825	1324.65	0.5878
D	0.6511	1576.63	0.7591
E	0.5092	1565.99	0.7082

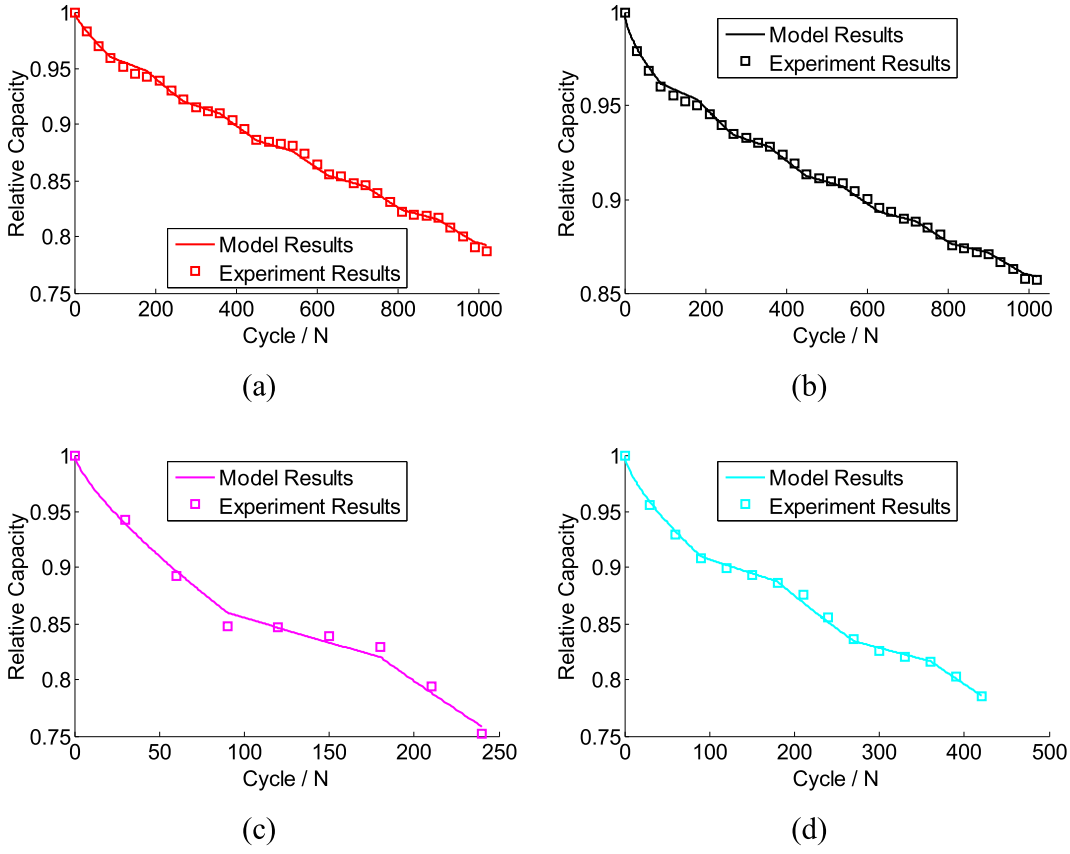

Fig. 5. Comparison of the simulated capacity fades and the experiment data. (a) Cell B, (b) cell C, (c) cell D, (d) cell E.

battery resistance is relatively easy to estimate. But the battery capacity is quite hard to estimate accurately because the battery SOC is hard to be accurately predicted, the cumulated Ampere-hours may have some errors, and so on. As shown in Fig. 6, cell D shows no big change in actual capacity within these several cycles. But the discharged capacity of every cycle is quite different. If those methods like dual Kalman filtering are used, the identified result would be that the cell capacity has dramatic fluctuation. The capacity loss model developed in Section 3 could be used, but: first, the battery cycle life test, which is designed to find the parameters of capacity loss model, require very long testing time; second, the parameter of capacity loss model fitted from the cells tested in the laboratory may be different from the cell used in the real vehicle because of the battery inconsistency; and third, without a feedback the estimation error may cumulated and the results would become unreliable. Therefore, at present a reasonable solution for batteries capacity loss estimation is model based open-loop capacity estimation with periodical capacity calibration and correction.

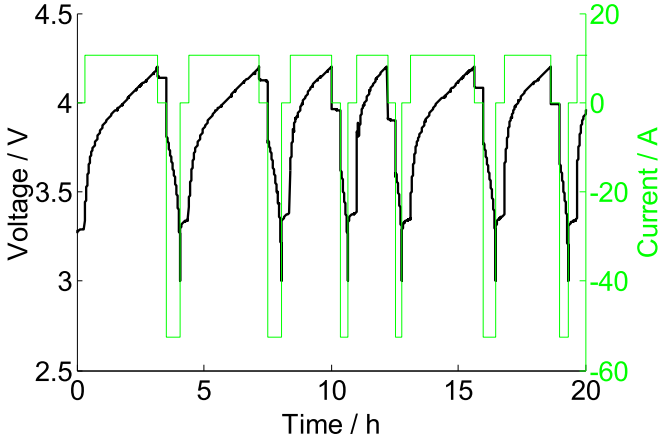

Fig. 6. The 211–216th cycles' voltage and current profiles of cell D, 45 °C.

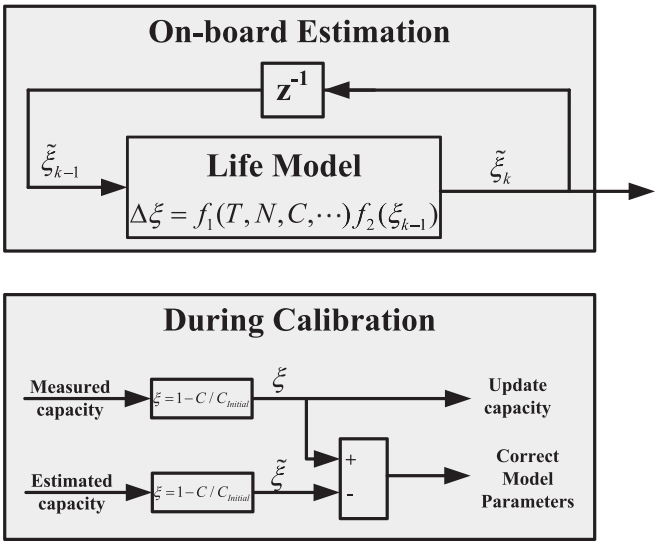

Fig. 7. Capacity estimation algorithm framework in BMS.

Table 3
Initial parameters of the cycle loss models of different batteries.

Battery type	A	E_a/R	z
C/LFP	0.15	1400	0.5
C/LMO	0.60	1400	0.5

A block diagram for the algorithm of battery capacity estimation is shown in Fig. 7.

As stated previously, the capacity loss of batteries can be described by semi-empirical models. The model introduced in Section 3 is simple and only the influence of temperature is considered, the influence of charge current, discharge current, etc., is not considered and thus more experiments are still needed. Generally, the discrete version of any semi-empirical model could be described as Eq. (13).

$$\xi_k = \xi_{k-1} + f_1(T,\ N,\ C,\ \ldots) f_2(\xi_{k-1}) \tag{13}$$

where the function f_2 represents the relationship between the next capacity loss and the existing batteries capacity loss ξ_{k-1}. The function f_1 represents the relationship between the battery capacity loss and the battery cycles. The input parameters of f_1 include temperature T, cycle number N, charge rate C, and so on. Thus using the cycle life model, the change of the battery capacity can be estimated in real time based on the battery working condition. Then the results could be used in such algorithms of SOC estimation, SOH estimation and energy management of batteries.

As shown in the Section 3, the parameters of battery capacity loss models for the same type of batteries are basically approximate. Therefore, the parameters of battery capacity loss model of the same type batteries can be considered the same. For a certain battery, the capacity loss model in the BMS may use the parameter which is tested before with another battery of the same type, but not the same capacity, even not the same manufactures. Meanwhile, batteries of the actual EVs shall be maintained regularly, and one of the important items is to calibrate the capacity. The regular calibration could not only update the latest battery capacity data to BMS, but also correct the parameters of the capacity loss models in the BMS by comparing the estimated capacity and the measured result and using the estimation error to feedback the model parameters. The feedback could use the method like the Luenberger observer, Kalman Filter, etc. Then the capacity loss model could adapt to different batteries with different capacity fade rates.

Consider the inconsistency among batteries and the different aging state, the most accurate method for battery capacity calibration is to disassemble and execute standard charge and discharge process for every single cell. But actually this method is quite hard to operate, since it requires great labor, long time and high costs. Therefore, a method which using the constant current charge voltage curves of each cell to find the capacity of every single cell in the battery packs during only one charging process could be used. The details of this method could be found in our previous work [29].

According to the aforesaid ideas, an analog simulation is executed in terms of the experimental results. Suppose the EV uses a certain type of lithium ion battery. Make open-loop estimation of the battery capacity based on the capacity loss models, calibrate the battery capacity once every half an operating year (that is, every 90 cycles), then feedback and correct the parameters of battery capacity loss models according to the error between the actual capacity of batteries and the simulated capacity from capacity loss model. Here for convenience, the feedback follows the idea of well known Luenberger observer and the parameters correction values are just proportional to the error. Cell D requires calibration of its capacity and correction of its parameters once every 30 cycles due to its poor performance and huge capacity fades. For the tested cycles, the battery capacity loss is considered to follow the Eq. (8) and the initial value of parameters of battery capacity loss models are shown in Table 3. The initial values of the model parameters given here are close but obviously different from the actual values. It is to simulate the situation that the capacity loss model parameters are unknown and to save the test time and cost, and the parameters are simply chosen according to the cathode and anode material.

Figs. 8–11 show the comparison between the estimated result of capacity and the tested values, the correction of modeling parameters and the changes of modeling errors. The real capacity of batteries can be obtained by interpolation according to the battery capacity obtained by testing.

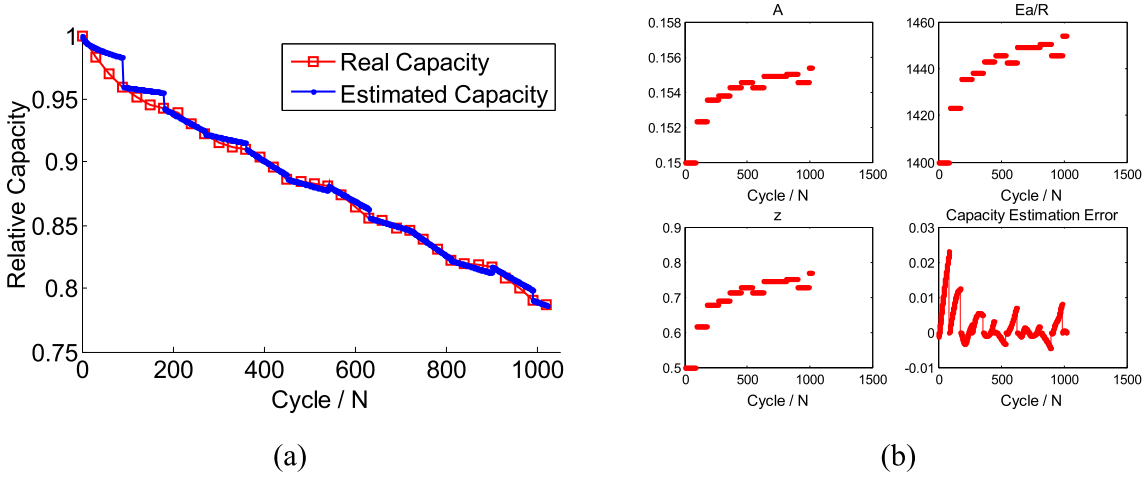

Fig. 8. Capacity estimation of cell B. (a) The real capacity and the estimated capacity; (b) the estimated parameters and capacity estimation error.

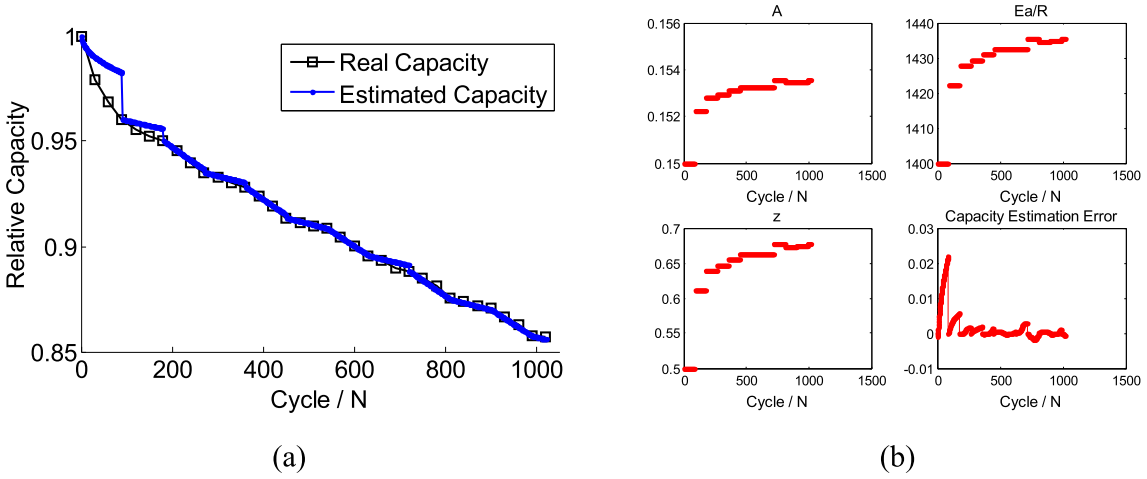

Fig. 9. Capacity estimation of cell C.

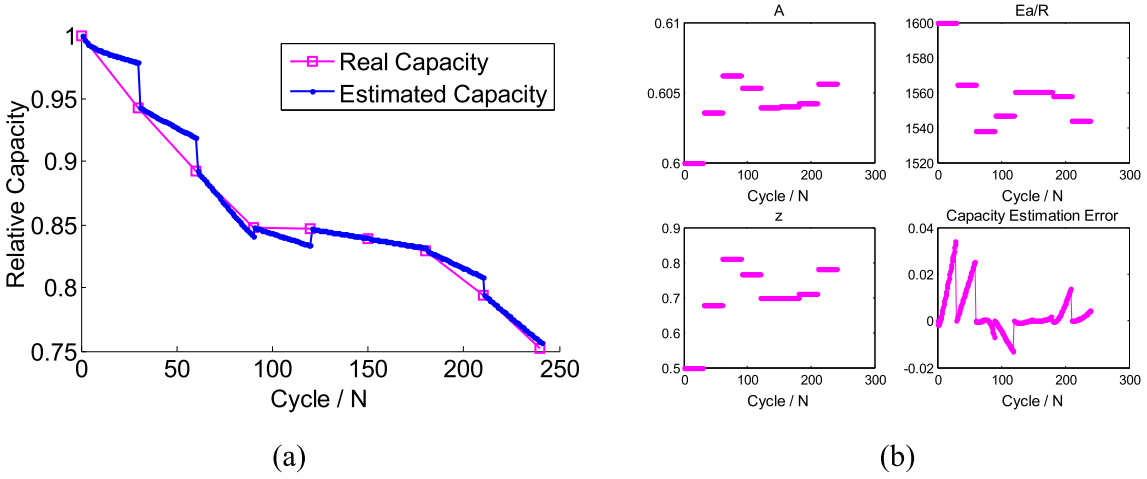

Fig. 10. Capacity estimation of cell D.

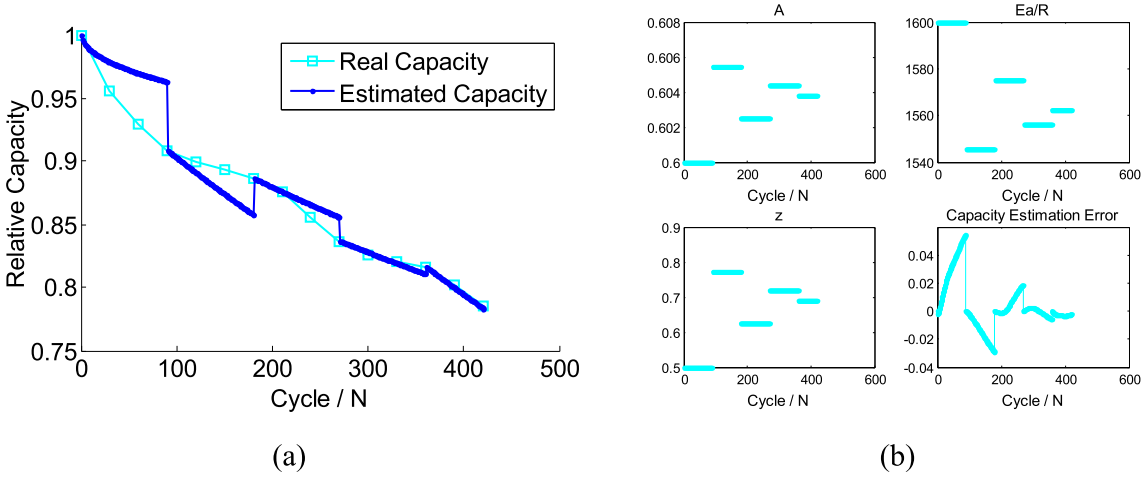

Fig. 11. Capacity estimation of cell E.

It can be seen that in the beginning the estimated results of capacity of all cells are poor, even leading to estimation error of up to 4% due to the difference between the given parameters of battery capacity loss models and the actual parameters. After every 90 cycles, the battery capacity is updated according to the calibration results and the model parameters are corrected. After several times of battery calibration, the BMS can eventually correct the model parameters and then the open-loop estimation errors of battery capacity could be controlled within 1% basically. This results show that the method introduced in this study could estimate the battery capacity precisely, while even the battery doesn't need to be tested and the capacity loss model parameters could be undetermined.

This experiment is conducted in the laboratory and the established results are obtained mainly based on such experiments. However, the actual on-board batteries may go through more complicated cycles. Such parameters of batteries in real vehicle as temperature and charge and discharge rate can be measured through the BMS and the cycle number N, etc., can be obtained by means of such cycle counting methods like rain flow counting method [30]. The battery capacity loss models still require further testing as well because more comprehensive battery capacity loss models can be further obtained by researching the capacity loss of batteries with different DODs (Depth of Discharge), charge and discharge rates, etc.

5. Conclusion

For pure EV, the cycle life of lithium ion batteries is of great importance. In this study, the cycle life test is designed according to the working condition of power batteries on the real EVs and taken on five different commercial lithium ion batteries. Consider that the batteries of pure EV works at different temperatures in different seasons, the selected cells are designed to cycle alternately under 45 °C and 5 °C. After 1020 times of cycles, it can be seen that the cycle life of LMO cells is very short, reaching the EOL after about 200 and 400 cycles respectively, and for LFP cells about 1000 more cycles. The cycle life of LTO batteries is very long. Then a battery capacity loss model is built to describe the battery capacity fades based on the identified battery aging mechanism and the literature, and transformed to a discrete version considering the dynamic cycles in this experiment and in the real vehicles. Using the experiment designed in this study, only one cell needs to be tested and the capacity loss model could be determined. The modeling results are proved to fit the experimental results precisely. And a novel method combined the on-line estimation and periodical calibration is proposed to on-board estimate the battery capacity loss. The estimation error of the battery capacity is less than 1%.

Acknowledgment

This research is funded by the MOST (Ministry of Science and Technology) of China under the contract of No. 2010DFA72760 and No. 2011AA11A227, the MOE (Ministry of Education) of China under the contract of No. 2012DFA81190, the Beijing Science and Technology Plan No. Z121100007912001, the National Support Plan 2013BAG16B01, and the Tsinghua University Initiative Scientific Research Program (Grand No. 2011Z01004).

Appendix A. Abbreviations

BMS	battery management system
C	carbon
CCCV	constant current–constant voltage
CD	charge-depleting
CPCV	constant power–constant voltage
CS	charge-sustaining
EV	electric vehicle
EOL	end of life
HPPC	Hybrid Pulse Power Characterization
HEV	hybrid electric vehicle
LFP	$LiFePO_4$
LMO	$LiMn_2O_4$
LTO	$Li_4Ti_5O_{12}$
NCM	$LiNi_xCo_yMn_{1-x-y}O_2$
MCCCV	multistage constant current–constant voltage
OCV	open circuit voltage
PHEV	plug-in hybrid electric vehicle
RMSE	rooted mean squared error
RPT	reference performance test
SEI	Solid Electrolyte Interface
SOC	state of charge
SOH	state of health

Appendix B. Battery performance evolution

With the battery cycle time increases, not only the battery capacity fades, but also the other battery performances change. The battery charge and discharge curves change and the battery resistance increases.

Fig. 12 shows the 1/3 C charge and discharge curves of the five cells at 25 °C after different cycle times from the capacity test data. It can be found that for cell A, the cell capacity almost keeps constant basically with increasing cycle number, but the charge curve and the discharge curve obviously alter. For cell B, the cell capacity clearly fades. The charge curve and the discharge curve change obviously, to be specific, the charge curves changes greatly at the end of charging, i.e., in the region with higher SOC, and changes little in other regions. For LFP cell C, it is similar to the LFP cell B. The charge curve changes obviously in the region with higher SOC. And at lower SOC region, the charge curves are almost same. For cell D, the charge curve and the discharge curve change greatly. With the increasing cycle time, the cell capacity fades dramatically, and the constant voltage charge section of the charging curves obviously increases. It could be easily found that the distance between the charge and discharge curves becomes longer, indicating that the resistance of the battery increases greatly. For cell E, the charge curve and the discharge curve also change obviously. The battery charging curves could be used to identify the cell aging mechanism by incremental capacity analysis, and the detailed aging mechanism identification results could be found in our previous work [23].

The battery resistance evolution is shown in Fig. 13. For simplification, here the 30 s discharge resistance of these 5 cells at SOC 50% after different cycles are plotted and compared. t can be seen that the resistance of all the 5 cells increased linearly basically. As mentioned previously, the capacity of LTO cell A, did not fade basically while it could be clearly seen that the resistance increased obviously. After 1020 cycles, the battery discharge resistance increased by about 20%. The LFP cell B lost about 20% of the initial capacity after 1020 cycles and the discharge resistance increased by about 35%. And after 1020 cycles, the capacity of the LFP cell C decrease by about 15% while the resistance shows almost no increment, the discharge resistance almost stay constant. The LMO cell E gets a 20% capacity loss and a 20% increment of discharge resistance after 420 cycles. By contrast, the situation of LMO cell D is very complicated. With increasing cycle number, its resistance increases greatly and the increment rate is much higher than the other cells. After 240 cycles, it almost increases to 4 times as much as the initial value.

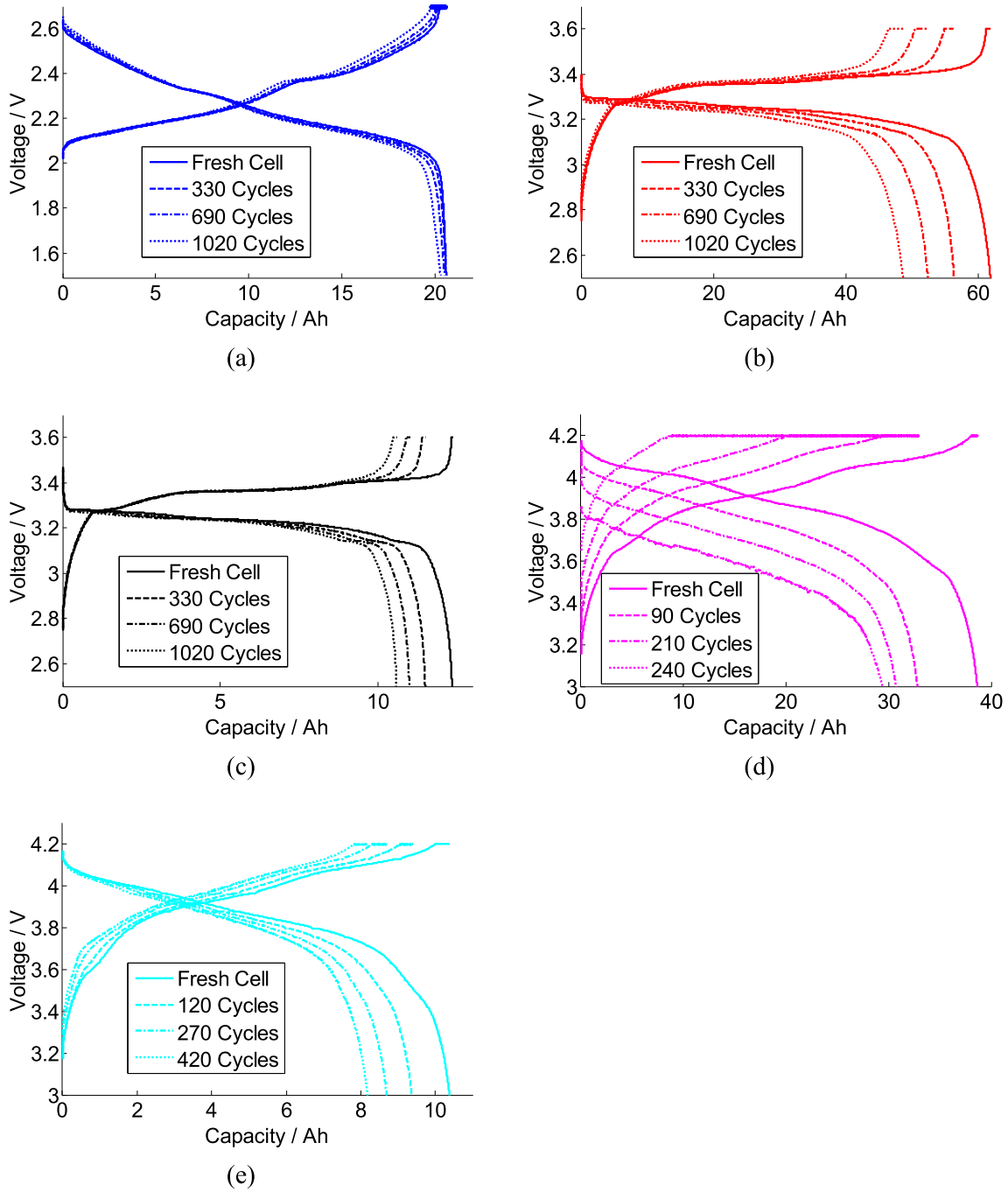

Fig. 12. Charge and discharge curves evolution of the five cells. (a), cell A; (b), cell B; (c), cell C; (d), cell D; (e), cell E.

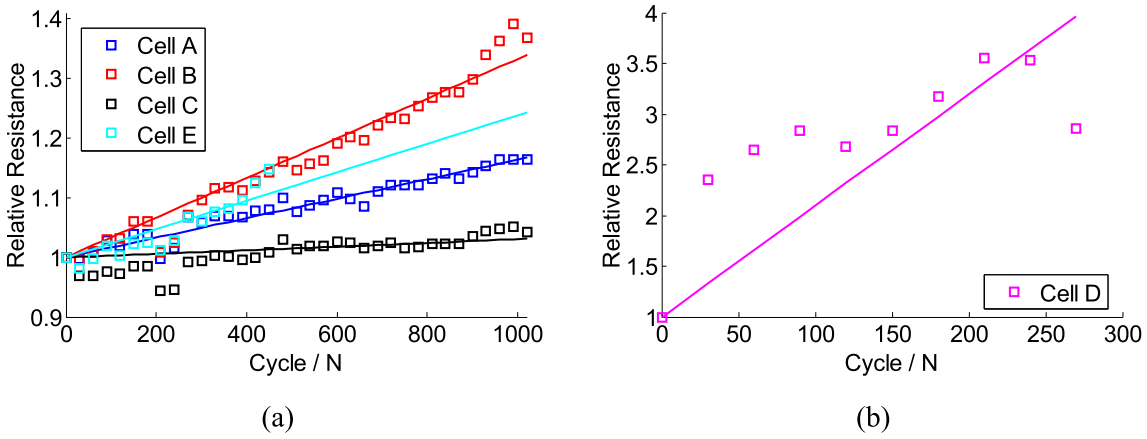

Fig. 13. Comparison of the relative 30 s discharge resistance evolution @50%SOC of different batteries. (a) cell A, B, C and E. (b) Cell D.

References

[1] L. Lu, X. Han, et al., J. Power Sources 226 (2013) 272–288.
[2] Bruno Scrosati, Jürgen Garche, J. Power Sources 195 (2010) 2419–2430.
[3] Jianming Zheng, Jie Xiao, Zimin Nie, Ji-Guang Zhang, J. Electrochem. Soc. 160 (8) (2013) A1264–A1268.
[4] P. Ramadass, Bala Haran, et al., J. Power Sources 112 (2002) 606–613.
[5] Sheng Shui Zhang, J. Power Sources 161 (2006) 1385–1391.
[6] Soo Seok Choi, Hong S. Lim, J. Power Sources 111 (2002) 130–136.
[7] Jiuchun Jiang, Wei Shi, Jianming Zheng, Pengjian Zuo, Jie Xiao, Xilin Chen, Wu Xu, Ji-Guang Zhang, J. Electrochem. Soc. 161 (3) (2014) A336–A341.
[8] I. Bloom, B.W. Cole, et al., J. Power Sources 101 (2001) 238–247.
[9] R.B. Wright, C.G. Motloch, et al., J. Power Sources 110 (2002) 445–470.
[10] J. Wang, P. Liu, et al., J. Power Sources 196 (2011) 3942–3948.
[11] J. Belt, V. Utgikar, I. Bloom, J. Power Sources 196 (2011) 10213–10221.
[12] M. Ecker, et al., J. Power Sources 215 (2012) 248–257.
[13] P. Ramadass, Bala Haran, et al., J. Electrochem. Soc. 151 (2) (2004) A196–A203.
[14] R. Spotnitz, J. Power Sources 113 (2003) 72–80.
[15] R. Deshpande, M. Verbrugge, Yang-Tse Cheng, J. Wang, P. Liu, 159 (10) (2012) A1730–A1738.
[16] Y. Dai, L. Cai, R.E. White, J. Power Sources 247 (2014) 365–376.
[17] Y. Dai, L. Cai, R.E. White, J. Electrochem. Soc. 160 (1) (2013) A182–A190.
[18] I. Bloom, B.W. Cole, J.J. Sohn, et al., J. Power Sources 101 (2001) 238–247.
[19] J. Wang, P. Liu, J. Hicks-Garnera, et al., J. Power Sources 196 (2011) 3942–3948.
[20] Toshio Matsushima, J. Power Sources 189 (2009) 847–854.
[21] N. Omar, M.A. Monem, Appl. Energy 113 (2014) 1575–1585.
[22] Z. Li, L. Lu, et al., J. Power Sources 196 (2011) 9757–9766.
[23] X. Han, M. Ouyang, L. Lu, J. Li, Y. Zheng, Z. Li, J. Power Sources 251 (2014) 38–54.
[24] Idaho National Engineering & Environmental Laboratory, Battery Test Manual for Plug-in Hybrid Electric Vehicles, September 2010. http://www.inl.gov/technicalpublications/Documents/4655291.pdf.
[25] USABC Electric Vehicle Battery Test Procedures Manual, Revision 2, Published January 1996, http://www.uscar.org/guest/article_view.php?articles_id=86.
[26] M. Safari, M. Morcrette, et al., J. Electrochem. Soc. 157 (6) (2010) A713–A720.
[27] H. Zheng, L. Zhang, G. Liu, X. Song, V.S. Battaglia, J. Power Sources 217 (2012) 530–537.
[28] S. Lee, J. Kim, J. Lee, B.H. Cho, J. Power Sources 185 (2008) 1367–1373.
[29] Y. Zheng, L. Lu, et al., J. Power Sources 226 (2013) 33–41.
[30] A. Nuhic, T. Terzimehic, et al., J. Power Sources 239 (2013) 680–688.